Magnetic characterization by SQUID and FMR of a biocompatible ferrofluid based on Fe_3O_4

2009 J. Phys.: Condens. Matter 21 115104

(http://iopscience.iop.org/0953-8984/21/11/115104)

J. Phys.: Condens. Matter **21** (2009) 115104 (6pp) doi:10.1088/0953-8984/21/11/115104

Magnetic characterization by SQUID and FMR of a biocompatible ferrofluid based on Fe_3O_4

L F Gamarra[1,2], W M Pontuschka[3], J B Mamani[3], D R Cornejo[3], T R Oliveira[3], E D Vieira[4], A J Costa-Filho[4] and E Amaro Jr[1,2]

[1] Instituto Israelita de Ensino e Pesquisa Albert Einstein, IIEPAE, 05651-901, São Paulo, Brazil
[2] Instituto de Radiologia, Faculdade de Medicina, USP, São Paulo, Brazil
[3] Instituto de Física, Universidade de São Paulo, São Paulo, Brazil
[4] Instituto de Física de São Carlos, USP, São Carlos, Brazil

E-mail: lgamarra@einstein.br

Received 17 July 2008, in final form 13 January 2009
Published 2 February 2009
Online at stacks.iop.org/JPhysCM/21/115104

Abstract

Biocompatible superparamagnetic iron oxide nanoparticles of magnetite coated with dextran were magnetically characterized using the techniques of SQUID (superconducting quantum interference device) magnetometry and ferromagnetic resonance (FMR).

The SQUID magnetometry characterization was performed by isothermal measurements under applied magnetic field using the methods of zero-field-cooling (ZFC) and field-cooling (FC). The magnetic behavior of the nanoparticles indicated their superparamagnetic nature and it was assumed that they consisted exclusively of monodomains. The transition to a blocked state was observed at the temperature $T_B = (43 \pm 1)$ K for frozen ferrofluid and at (52 ± 1) K for the lyophilized ferrofluid samples. The FMR analysis showed that the derivative peak-to-peak linewidth (ΔH_{PP}), gyromagnetic factor (g), number of spins (N_S), and spin–spin relaxation time (T_2) were strongly dependent on both temperature and super-exchange interaction. This information is important for possible nanotechnological applications, mainly those which are strongly dependent on the magnetic parameters.

(Some figures in this article are in colour only in the electronic version)

1. Introduction

Iron oxide nanoparticles are of considerable interest for applications in nanotechnology due to their inherent properties, such as superparamagnetism, high saturation fields, and extra anisotropy contributions or shifted loops after field-cooling, which is attributed to finite size and large surface area [1]. Currently these nanostructured materials are applied in various fields such as magnetic storage, biomedicine, and catalysis [2–4].

The magnetic characterization of superparamagnetic iron oxide nanoparticles (SPIONs) having different physical–chemical configurations is fundamental in medical applications, including drug delivery [5], and hyperthermia cancer treatment [6, 7], among others. They are also used as image contrast agents in magnetic resonance imaging (MRI) [8, 9], where the principle of this application is based on the magnetic properties of the SPIONs. The physical properties of an assembly of magnetically ordered monodomains in a diamagnetic matrix depend on a number of parameters which characterize the magnetic compound and on the morphology of the nanoparticles. Such systems of superparamagnetic nanoparticles are currently being investigated by a large variety of techniques, where the main goals are to further explore the properties of these materials and to increase their potential for novel applications, taking into account that each potential application requires different properties of the nanoparticles.

The objective of this paper is to perform the magnetic characterization of a colloidal suspension of SPIONs recovered with dextran used as a contrast agent for MRI. The magnetic characterization was performed using the techniques of superconducting quantum interference device (SQUID)

magnetometry and ferromagnetic resonance (FMR). The FMR analysis was carried out as a function of temperature in order to understand the superparamagnetic features exhibited by the SPIONs under investigation, as well as the temperature dependence of parameters such as the peak-to-peak linewidth, gyromagnetic factor, number of spins and spin–spin relaxation time.

1.1. Ferromagnetic resonance

Electron paramagnetic resonance (EPR) of the ferromagnetic particles, also known as FMR, is performed like any other EPR experiment, except that the samples contain approximately spherical aggregates of ferro or ferrimagnetic monodomains of the order of a few nanometers. Thus, the total magnetic momentum of each nanoparticle precesses about the direction of the total magnetic static field, which is the sum of the external static field, the internal contribution of the domain magnetization and the anisotropic magnetic field of the local lattice [10]. The FMR is adequate for the study [11] and detection of ferromagnetic nanoparticles [12, 13] even in the presence of soluble iron salts, which exhibit typical well-defined spectra.

The magnetic resonance theory of the superparamagnetic systems is described on the basis of a phenomenological equation of motion for a classical magnetic momentum $\boldsymbol{\mu}$ under ferromagnetic conditions of resonance [14, 15].

The magnetic fluids based on SPION present various relaxation phenomena, which are directly related to the orientation freedom degrees of the particle. The basic phenomenon of FMR is the microwave absorption, which is observed when the Larmor precession of the particles equals the frequency of the standing waves in the microwave cavity. The physical mechanism is essentially the same for ferromagnetic solids and magnetic suspensions. However, in ferrofluids, the FMR is considerably affected by two specific characteristics. The first one stems from the smallness of the particles and imparts a fluctuation component to the magnetic moment motion. The second originates from the mechanical mobility of the particles and results in a change in the distribution of their anisotropy axes under the influence of the external fields [16]. The underlying cause of both effects is the thermal noise, meaning that they are strongly temperature-sensitive.

Among the nanoparticles composed by spherical monodomains (∼10 nm), the reference value KV of the magnetic anisotropic energy, where K is the constant of anisotropy and V is the particle volume, can be easily compared with the thermal energy $k_{\mathrm{B}}T$. Because of this, together with any regular movement, the magnetic momentum $\boldsymbol{\mu}$ of the particle is submitted to considerable orientation fluctuations, including those that reverse their direction. This effect is known as superparamagnetism and it was predicted by Néel [17].

2. Materials and methods

The sample was a colloidal suspension of iron oxide superparamagnetic nanoparticles (Endorem™—Guerbert, earlier trade name AMI-25, Laboratoire Guerbert, France) consisting of 126.500 mg of Fe_3O_4 superparamagnetic nanoparticles contained in 8 ml of water. The nanoparticles of 4.8–5.6 nm size are coated with low-weight dextran (7–9 kDa) [18] of hydrodynamic diameters between 80 and 150 nm. Besides water, the solvent composition was 60.800 mg of dextran, 2.714 mg of citric acid, and 490.400 mg of β-D-mannitol ($C_6H_{14}O_6$). The pharmacokinetics, toxicity, and relaxivity of these superparamagnetic iron oxide particles have been previously described [19–21]. The suspension is a ferrofluid applied as a contrast agent in MRI for the detection of liver lesions associated with an alteration in the reticular-endothelial system (RES) [9].

The magnetic characterization was performed by SQUID magnetometry and FMR. A commercial SQUID magnetometer was employed to perform static and dynamic measurements as a function of field, temperature, and driving frequency. Zero-field-cooling (ZFC) and field-cooling (FC) curves were recorded under applied magnetic fields up to 7 T, between 5 and 250 K to avoid the melting of the solid matrix (solvent). The study using this technique was carried out with two types of ferrofluid samples: (a) as a colloidal suspension and (b) as a lyophilized ferrofluid in order to increase the concentration of nanoparticles, keeping their size unaltered. The samples were lyophilized on an Edwards lyophilizer, model E3M8-Modulyo, operating at a temperature of $-50\,^{\circ}$C and pressure of 8×10^{-3} Torr, working with a vacuum pump. This process was carried out during a period of 27 h, yielding a material free of humidity.

For magnetic measurements, as-prepared samples were conditioned in closed containers before quenching the magnetite/carrier mixture below its freezing point (∼268 K).

The FMR spectra were obtained using a Bruker ELEXSYS E580 spectrometer operating at X band (9.2 GHz) and equipped with a rectangular microwave cavity operating in the TE_{102} mode. Experimental parameters were set to avoid saturation and distortion of the signal. To obtain the FMR spectra in the temperature range of 4–300 K, 3.5 mM of SPIONs colloidal suspension sample in a volume of 10 μl was used. The temperature was controlled by an ITC503 Oxford cryostat system.

3. Results and discussions

Magnetization curves (figure 1) obtained from SQUID magnetometry measurements, taken in ZFC and FC modes under an external field of $H = 100$ Oe showed that the transition to a blocked state occurs at the temperature $T_{\mathrm{B-F}} = (43 \pm 1)$ K for frozen ferrofluid. On the other hand, it can be clearly seen that the lyophilized ferrofluid sample had a higher blocking temperature $T_{\mathrm{B}} = (52 \pm 1)$ K. At the irreversibility temperature (T_{Irr}) splitting of the ZFC and FC curves was observed when the larger particles were changed from the blocked state to the superparamagnetic state and vice versa. For the case of the lyophilized ferrofluid and the frozen ferrofluid sample, the following values $T_{\mathrm{Irr-L}} = (97 \pm 1)$ K and $T_{\mathrm{Irr-F}} = (220 \pm 1)$ K were observed, respectively. The changes in the temperatures T_{B} and T_{Irr} showed the

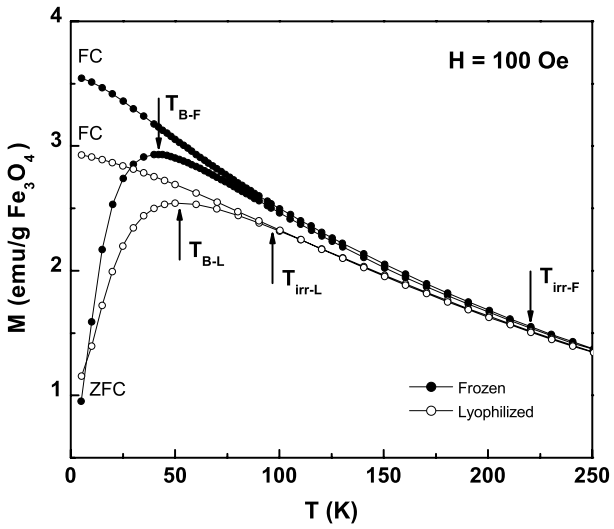

Figure 1. Magnetization curve for frozen (●) and lyophilized (○) samples. Lower and upper branches correspond to ZFC and FC data, respectively. The arrows indicate the blocking temperature T_B and the irreversibility temperature T_{irr}.

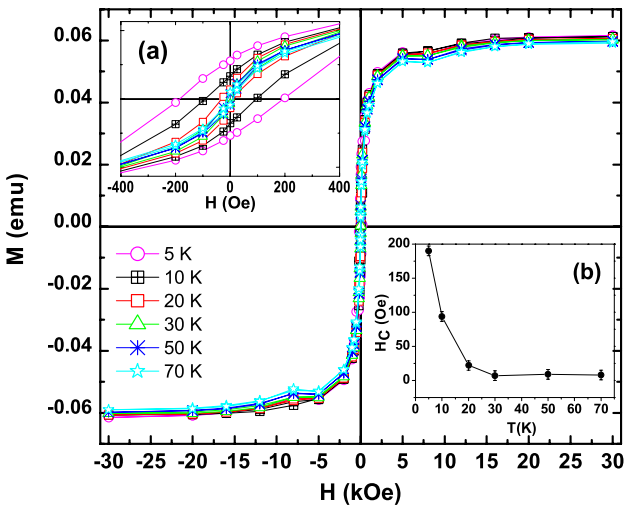

Figure 2. Hysteresis cycles of the ferrofluid at different temperatures. Inset (a): detail showing the reminiscent field with a field range from −400 to +400 Oe. Inset (b): coercive fields measured in the blocking region of the ferrofluid sample.

effects of dipolar interactions, which tend to increase the energy barriers of individual particles. According to the size of monodomain particles, no indication of the Verwey transition was observed. By comparing samples with different average particle distances but identical particle distributions, we inferred that in concentrated systems the contribution from dipolar interactions can be of the same order as the anisotropy energy barriers of noninteracting particles.

Contributions to anisotropy energy can originate from intrinsic anisotropies of the particles (shape, magnetocrystalline, or stress anisotropies) or interparticle interactions (dipolar or exchange). Inasmuch as these two mechanisms contribute to modify the energy barrier, it is usually quite difficult to separate both kinds of effects. The conditions during the lyophilization assured that both samples have the same average particle size, particle distribution, and particle shape. Therefore, such an increase in anisotropy energy is not related to size/distribution effects but to the decrease of the average distance between particles.

Figure 2 shows the hysteresis cycles for the ferrofluid samples measured at temperatures of 5, 10, 20, 30, 50, and 70 K. It is well known that after the initial magnetization, the sample acquires a remnant magnetization even after the removal of the external field. The field necessary to further reduce the remnant magnetization to zero is defined as the coercive field H_c, which is calculated from the hysteresis curve (figure 2(a)). Figure 2(a) shows the existence of coercive field at temperatures below the blocking temperature. Thus, it is also observed that the material has a typical superparamagnetic behavior, i.e. with almost zero coercivity, because during the time elapsed in the measurement (τ_m), the particles are in the superparamagnetic state at temperatures higher than the blocking temperature (T_B). As the temperature of the system decreases, the hysteresis appears and consequently the superparamagnetism disappears, where the thermal energy is no longer sufficient to overcome the potential barrier created by the anisotropic energy, thereby blocking their magnetic moments during the time τ_m.

The $M(H)$ curves shown in figure 2(a) indicate the development of a measurable coercive field below T_B, reaching the field intensity $H_C = 190$ Oe for the temperature $T = 5$ K (see figure 2(b)). The saturation magnetization M_S is almost reached for applied fields of the order of 30 kOe, suggesting no evidence of a magnetically hard particle surface, as found in other nanostructured iron oxide particles [22]. The ratio between the saturation and the remnant magnetization $R = M_R/M_S$ measured at 5 K is 0.27, smaller than the theoretically expected $R = 0.5$ value for noninteracting randomly oriented particles [23]. It has been suggested that $R > 0.5$ and $R < 0.5$ values should be expected for those systems with ferro and antiferromagnetic interactions, respectively, as proposed by Hadjipanayis *et al* [24]. Thus, the present $R = 0.27$ value indicates that the interparticle interactions are of antiferromagnetic nature.

The FMR spectrum at room temperature of ferrofluid is shown in figure 3. The typical ferrofluid spectra consisted of a broad line. The characteristic FMR absorption line of precipitated fine grains, composed by ferro-or antiferromagnetic monodomains [25, 26], is also observed in pairs of iron ions (Fe^{3+} and Fe^{2+}) and/or clusters formed in glassy matrices [27]. From the lineshape analysis it was possible to determine the magnetocrystalline anisotropic constant of first order $K_1 = (1.2 \pm 0.2) \times 10^5$ erg cm^{-3}, following a method described in the literature [25]. This value was determined by using the relations $H_a = 2K_1/M_S$ and $H_S = (4\pi/3)M_S$ (erg G^{-1} cm^{-3}), where $H_S \approx 2$ kG [25]. It was considered that the SPIONs chemical composition is Fe_3O_4 [25], consisting of monodomains of spherical geometry [26]. M_S is the magnetization saturation of the cubic crystal and H_S is the saturation field of a spherical SPION. The derivative of FMR absorption shows a maximum H_{max}, a minimum H_{min}, and a maximum of negative slope

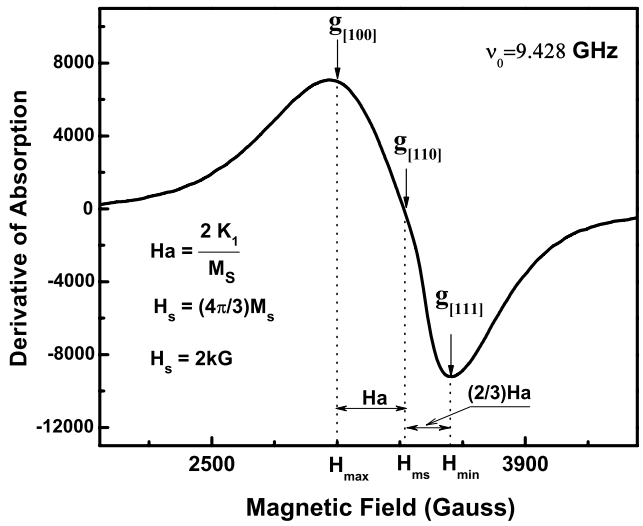

Figure 3. FMR spectrum of SPIONs recorded at room temperature.

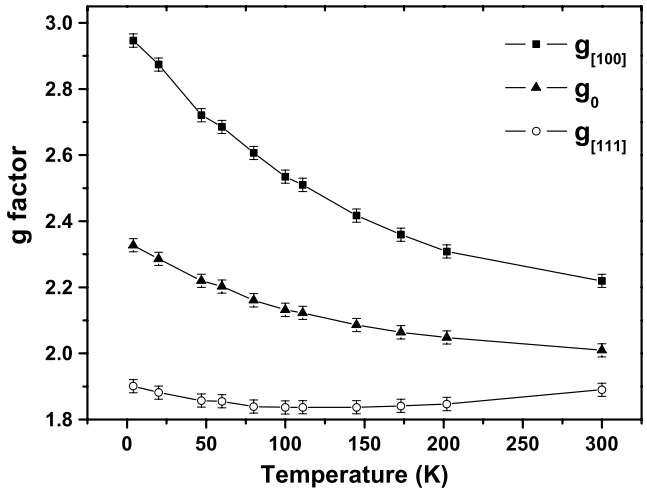

Figure 5. Temperature dependence of the gyromagnetic factors $g_{[100]}$, g_0, $g_{[111]}$ of SPIONs.

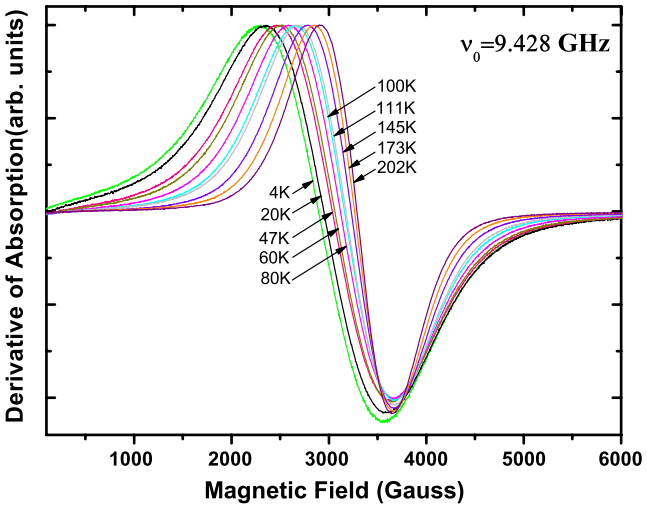

Figure 4. Temperature dependence of the ferrofluid FMR spectra obtained in the range of 4–300 K.

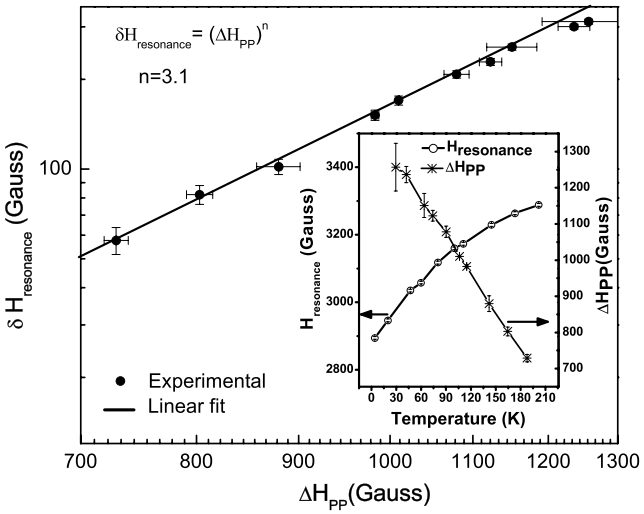

Figure 6. Relationship between $\delta H_{\text{resonance}}$ and ΔH_{PP}, showing an exponent n of order 3. In the inset, the variation of $H_{\text{resonance}}$ and ΔH_{PP} as a function of temperature is illustrated.

H_{ms} whose values of effective g are $g_{[100]} = (2.22 \pm 0.01)$, $g_{[110]} = (1.98 \pm 0.02)$, and $g_{[111]} = (1.89 \pm 0.01)$, respectively. The H_a value was obtained from the field separation between the wing positions of H_{max} and H_{min}, equal to 5/3 of H_a, as shown in figure 4. The $H_0 = H_{\text{max}} - (2/3)H_a$ was obtained from the value of $g_0 = (h\nu/(\beta H_0)) = (2.01 \pm 0.02)$, with $\nu = 9.428$ GHz, where h is the Planck's constant, ν is the spectrometer microwave frequency and β is the Bohr magneton.

FMR measurements were carried out at varying temperatures from 4 K up to room temperature as shown in figure 4. In general, the spectra were asymmetric and the peak-to-peak amplitude of the derivative of absorption remained constant through the entire temperature range. However, a lineshape change was observed as temperature increased, leading to successively narrower lines. This is due to the fact that in a ferromagnetic randomly oriented dispersion, the absorption linewidth turns out to be a monotonic function of temperature. At low temperature, the linewidth is large due to the particle dispersion in the direction of the anisotropic field. As the temperature increases, there is a tendency of isotropic magnetic moments to be formed, thus reducing the linewidth [28].

The gyromagnetic factors $g_{[100]}$, g_0 of SPIONs decreased monotonically with temperature, and in the case of $g_{[111]}$ it starts with a slight decrease, reaching a minimum at 150 K and then increases slowly, as shown in figure 5.

In figure 6, the shift of the resonance field ($\delta H_{\text{resonance}} = [H_{\text{resonance}}]_{300\text{ K}} - [H_{\text{resonance}}]_T$) is plotted versus the peak-to-peak linewidth ($\Delta H_{\text{PP}} = H_{\text{min}} - H_{\text{max}}$) of the FMR spectrum (derivative of the microwave absorption), and a straight line was obtained assuming that the function is nth power of ΔH_{PP}. The inset shows the decrease of resonance field with the increase in temperature. $H_{\text{resonance}}$ is plotted versus ΔH_{PP} and it also shows the dependence of ΔH_{PP} with the associated temperature. The curve $H_{\text{resonance}}(T)$ increase with the increase

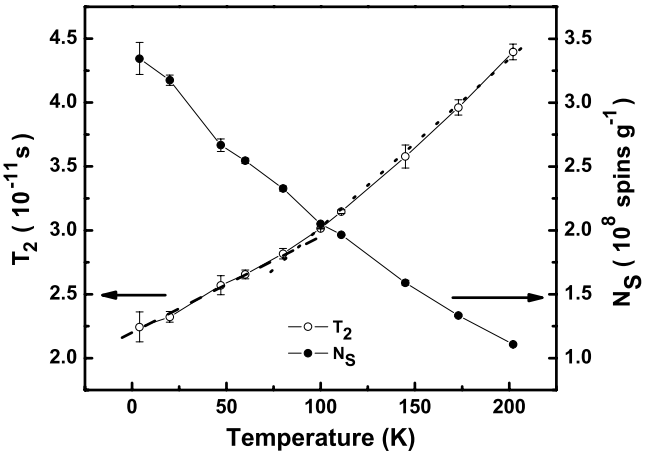

Figure 7. The spin–spin relaxation time (T_2) and the spin number as a function of temperature of ferrofluid.

in temperature, whereas ΔH_{PP} decreases with the increase in temperature, as expected for the FMR of superparamagnetic particles [29, 30]. Therefore, it is expected that the resonance line broadening should be associated with the magnetization blocking of the Fe_3O_4 nanoparticles.

The variation of ΔH_{PP} can be explained using a two-level system and assuming thermal equilibrium. The FMR linewidth is given by [31]

$$\Delta H_{PP} = L \tanh\left[\frac{\Delta E}{2kT}\right], \qquad L = \frac{5g\beta Sn}{D^3} \tag{1}$$

where n is the number of magnetic centers, g is the gyromagnetic factor, D is the average intergrain distance, S is the effective spin of the magnetic centers and ΔE is the energy barrier. Therefore, L remains unchanged and the main contribution to ΔH_{PP} would be ΔE. The weakening of the magnetic coupling is the possible reason for the observed decrease in the linewidth [30, 32].

In general, for a system of superparamagnetic particles with statistical distribution of shapes and sizes, there is a simple relationship between n, the exponent of $\delta H_{\text{resonance}} \sim (\Delta H_{PP})^n$, and the structural organization of the particles [33]: $n = 2$ for partially oriented and $n = 3$ for randomly oriented particles. To examine this power relationship, the data were plotted as shown in figure 6 on a double logarithmic scale. From the adjusted slope of $n \sim 3(3.1)$, it is concluded that the behavior of the magnetite nanoparticles is superparamagnetic, isolated, and randomly oriented.

The number of unpaired electron spins in the sample is proportional to the area under the absorption of FMR, determined by $(\Delta H_{PP})^2\Gamma$ where Γ is the peak-to-peak height [34]. It is seen in figure 7 that the number of spins decreased with the increase of temperature.

The spin relaxation process is characterized using a time constant which is a function of the static magnetic field and is dependent on the rate of absorption and dissipation of the microwave energy. The spin–spin relaxation process is the energy difference ΔE transferred to the neighboring electrons. The relaxation time T_2 can be determined from the peak-to-peak linewidth according to the following equation, expressed in units s^{-1}:

$$\frac{1}{T_2} = \frac{\sqrt{3}g\beta\Delta H_{PP}}{\hbar}, \tag{2}$$

where $\hbar$ is the Planck's constant divided by 2π.

Figure 7 shows the variation of T_2 with temperature. The dipole–dipole interaction between the particles and the super-exchange interaction between the magnetic ions through oxygen ions are the two predominant factors which determine the resonance parameters: the gyromagnetic g-factor and ΔH_{PP}. Strong dipolar interactions result in high values of ΔH_{PP} and g-factor. In addition, a strong super-exchange interaction produces small values of ΔH_{PP} and g-factor [35]. The increase of temperature should increase the motion of electrons, causing a stronger super-exchange interaction between the cations through oxygen ions and thus a decrease in ΔH_{PP} and g-factor. Consequently, T_2 increases with the increase in temperature. Another interesting observation is the change of the $\log \delta H$ slope with temperature, as shown in figure 7, with evidence of two types of relaxation rates. The change in the relaxation rate of the superparamagnetic iron oxide at $T = 75$ K can be related with the change of magnetic susceptibility [36]. The immediate interpretation is the change from a partially oriented to a randomly oriented spin behavior. It is closely analogous to the behavior of a glass crossing the glass transition temperature T_g, but this phenomenon needs further investigation.

4. Conclusion

From the ZFC and FC magnetization measurements, the transition to a blocked state was observed at the temperature $T_B = (43 \pm 1)$ K for frozen ferrofluid and at (52 ± 1) K for the lyophilized ferrofluid samples, showing the effects of dipolar interactions in distributions of samples with identical size. The magnetization results as a function of the external field showed that for temperatures $T > T_B$ the hysteresis cycle did not exhibit coercivity, indicating the superparamagnetic behavior of the material. However, on cooling below the blocking temperature, the magnetization of the sample increased and the hysteresis cycle became symmetric, showing a phase transition from the superparamagnetic to the ferromagnetic state.

The analysis of the FMR spectra of the ferrofluid measured in the range of temperatures 4–300 K confirmed the superparamagnetic state above T_B and the strong dependence of the parameters ΔH_{PP}, g-factor, N_S, and T_2 on temperature. It is known that this behavior of the measured parameters is strongly governed by super-exchange interaction.

Acknowledgments

This work was supported by Instituto Israelita de Ensino e Pesquisa Albert Einstein and the Brazilian agencies FAPESP and CNPq.

References

[1] Batlle X and Labarta A 2002 *J. Phys. D: Appl. Phys.* **35** R15
[2] Weller D, Sun S H, Murray C, Folks L and Moser A 2001 *IEEE Trans. Magn.* **37** 2185
[3] Bulte J W, Douglas T, Mann S, Frankel R B, Moskowitz B M, Brooks R A, Baumgarner C D, Vymazal J, Strub M P and Frank J A 1994 *J. Magn. Reson. Imaging* **4** 49
[4] Bell A T 2003 *Science* **299** 1688
[5] Voltairas P A, Fotiadis D I and Michalis L K J 2002 *Biomechanics* **35** 813
[6] Jordan A, Scholz R, Wust P, Fahling H, Krause J, Wlodarczyk W, Sander B, Vogl T and Felix R 1997 *Int. J. Hyperth.* **13** 587
[7] Shinkai M, Yanase M, Suzuki M, Honda H, Wakabayashi T, Yoshida J and Kobayashi T 1999 *J. Magn. Magn. Mater.* **194** 176
[8] Jordan A, Scholz R, Wust P, Fahling H and Felix R 1999 *J. Magn. Magn. Mater.* **201** 413
[9] Wang Y X J, Hussain S M and Krestin G P 2001 *Eur. Radiol.* **11** 2319
[10] Shilov V, Raikher Yu L, Bacri J C, Gazeau F, Perzynski R and Stepanov V I 1998 *Phys. Rev.* B **60** 11902–5
[11] Gazeau F, Shilov V, Bacri J C, Dubois E, Gendron F, Perzynski R, Raikher Yu L and Stepanov V I 1999 *J. Magn. Magn. Mater.* **202** 535–46
[12] Iannone A, Magin R L, Walczak T, Federico M, Swartz H M, Tomasi A and Vannini V 1991 *Magn. Reson. Med.* **22** 435–42
[13] Wilhelm C, Gazeau F and Bacri J C 2002 *Eur. Biophys.* **31** 118–25
[14] Raikher Y L and Stepanov V I 1992 *Sov. Phys.* **75** 764
[15] Raikher Y L and Stepanov V I 1994 *Phys. Rev.* B **50** 6250
[16] Raikher Y L and Stepanov V I 1995 *J. Magn. Magn. Mater.* **149** 34
[17] Néel L 1949 *Ann. Geophys.* **5** 99
[18] Laniado M, Chachuat A and Verträglichkeitsprofil von ENDOREM 1995 *Radiologe* **35** (Suppl. e) S266
[19] Halavaara J T, Lamminen A E, Bondestam S, Standertskjoeld-Nordenstam C G and Hamberg L M 1994 *J. Comput. Assist. Tomogr.* **18** 897–904
[20] Weissleder R, Stark D D, Engelstad B L, Bacon B R, Compton C C, White D L, Jacobs P and Lewis J 1989 *Am. J. Roentgenol.* **152** 167
[21] Majumdar S, Zoghbi S S and Gore J C 1990 *Invest. Radiol.* **25** 771
[22] Stoner E C and Wohlfarth E P 1948 *Phil. Trans. R. Soc.* **240** 599
[23] Goya G F, Berquo T S, Fonseca F C and Morales M P 2003 *J. Appl. Phys.* **94** 3520
[24] Hadjipanayis G, Sellmyer D J and Brandt B 1981 *Phys. Rev.* B **23** 3349
[25] Griscom D L 1984 *J. Non-Cryst. Solids* **67** 81
[26] Ray C S, Reis S T, Pontuschka W M, Yang J B, Sene F F, Giehl J M, Kim C W and Sen S 2006 *J. Non-Cryst. Solids* **352** 3677
[27] Reis S T, Faria D L A, Martinelli J R, Pontuschka W M, Day D E and Partiti C S M 2002 *J. Non-Cryst. Solids* **304** 189
[28] Massart R, Zins D, Gendron F, Rivoire M, Mehta R V, Upadhyay R V, Goyal P S and Aswal V K 1999 *J. Magn. Magn. Mater.* **201** 73
[29] Stucki J W and Banwart W L 1980 *Advanced Chemical Methods for Soil and Clay Mineral Research* (Dordrecht: Reidel)
[30] Kinnari P, Upadhyay R V and Mehta R V 2002 *J. Magn. Magn. Mater.* **252** 35
[31] Tronconi A L, Moris P C, Pelegrini F and Tourinho F A 1992 *J. Magn. Magn. Mater.* **122** 90
[32] Kinnari P, Upadhyay R V, Mehta R V and Srinivas D 2002 *J. Appl. Phys.* **88** 2799
[33] Nagata K and Ishihara A 1992 *J. Magn. Magn. Mater.* **1571** 104–7
[34] Raber J F 1980 *Experimental Methods in Polymer Chemistry—Physical Principal and Applications* (New York: Wiley) p 332
[35] Li L, Li G, Smith R L and Inomata H 2000 *Chem. Mater.* **12** 3705
[36] Wu K H, Chang Y C, Chen H B, Yang C C and Horng D N 2004 *J. Magn. Magn. Mater.* **278** 156